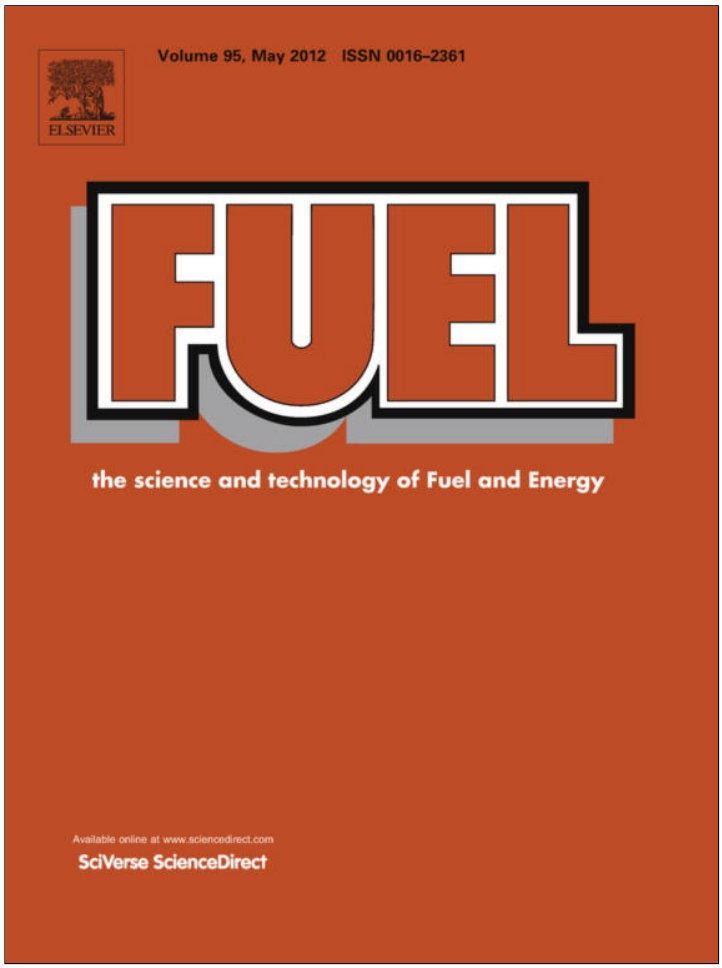

Fuel 95 (2012) 234–240

Contents lists available at SciVerse ScienceDirect

Fuel

journal homepage: www.elsevier.com/locate/fuel

Laminar burning characteristics of 2,5-dimethylfuran and *iso*-octane blend at elevated temperatures and pressures

Xuesong Wu [a,b], Qianqian Li [a], Jin Fu [a], Chenglong Tang [a], Zuohua Huang [a,*], Ritchie Daniel [b], Guohong Tian [b,c], Hongming Xu [b]

[a] State Key Laboratory of Multiphase Flow in Power Engineering, Xi'an Jiaotong University, Xi'an 710049, China
[b] Future Power System Group, University of Birmingham, Birmingham B15 2TT, United Kingdom
[c] Sir Joseph Swan Centre, Newcastle University, Newcastle upon Tyne NE1 7RU, United Kingdom

ARTICLE INFO

Article history:
Received 29 June 2011
Received in revised form 11 October 2011
Accepted 29 November 2011
Available online 11 December 2011

Keywords:
2,5-Dimethylfuran
Iso-octane
Laminar flame speed
Markstein length
Flame instability

ABSTRACT

2,5-Dimethylfuran, known as DMF, is a promising second-generation biofuel candidate. The potential of 2,5-dimethylfuran as an additive in *iso*-octane (used as gasoline fuel substitute in this study) was studied. Using outwardly spherical flame method and high speed schlieren photography, laminar burning characteristics of 2,5-dimethylfuran/*iso*-octane (20%/80% vol., designated as D20)/air mixtures were experimentally investigated. Laminar flame speeds and Markstein lengths of D20–air mixtures were empirically organized as a function of initial pressures and temperatures. Onset of cellular structures at the flame front was observed at relatively higher initial pressures due to the combined effect of diffusional-thermal and hydrodynamic instabilities. Laminar flame speeds of D20–air mixtures are higher than those of *iso*-octane–air mixtures when the equivalence ratio is greater than 1.2.

1. Introduction

2,5-Dimethylfuran (DMF), which can be massively produced from non-food biomass [1–3], has been regarded as a promising second-generation biofuel candidate. Compared to ethanol (the favored gasoline-alternative biofuel), DMF has a higher energy density, a higher boiling point and a higher research octane number (RON) [1,4]. It is insoluble in water, thus will not contaminate underground water during production or storage. It has the potential to become an alternative to fossil fuels and octane improver.

Most of previous work focused on the fundamental combustion characteristics [5–7] of DMF. Possible reaction pathways of DMF were proposed by Wu et al. [8] using the experimentally measured flame structure of the low-pressure premixed laminar DMF–O_2–Ar flame with tunable vacuum ultraviolet synchrotron radiation photoionization and molecular-beam mass spectrometry. Practically, Zhong et al. [9] studied the engine performance and emissions of DMF at fixed spark timing regardless of load in a direct-injection spark-ignition single cylinder research engine. Daniel et al. [10] compared the engine performance and emissions of DMF, gasoline and ethanol under gasoline MBT ignition timing and fuel-specific ignition timing in the same engine. These engine studies suggest that the resistance of DMF to knock is not as high as expected and lower than that of ethanol. Wu et al. [11] studied the flexible, bi-fuel concept – dual-injection strategy on a spark-ignition engines fueled with various gasoline, DMF and ethanol blends and they proposed that dual-injection strategy is a promising engine concept.

Laminar flame speed is an important fundamental physico-chemical property of a fuel–air mixture, which can be used to validate the chemical reaction mechanisms and to gain a better understanding of the combustion process, such as the turbulence combustion in SI engines and power generation systems [12]. Wu et al. [13–15] studied the laminar flame speeds, Markstein lengths and flame instabilities of DMF–air premixed mixtures at elevated temperatures and pressures over a wide range of equivalence ratios. Tian et al. [16] studied the flame propagation characteristics of DMF using the schlieren optical method. They found that the laminar flame speed of DMF was very similar to gasoline and the difference was within 10% in the equivalence ratio range 0.9–1.1.

Practical options of using DMF as engine fuel should consider it as an additive to primary fuel so as to avoid large modifications of the combustion devices. *Iso*-octane is widely used as gasoline alternate in fundamental combustion study. Thus, it is necessary to study the laminar combustion characteristics of DMF and *iso*-octane blend, which are important for assessing the possibility of DMF as an alternative for fossil fuels or octane improver. Laminar flame speed is useful for the analysis and performance predictions of various spark ignition engines. The objective of the present work is to provide fundamental laminar flame data of DMF and *iso*-octane

* Corresponding author. Tel.: +86 029 82665075; fax: +86 029 82668789.
E-mail address: zhhuang@mail.xjtu.edu.cn (Z. Huang).

0016-2361/$ - see front matter © 2011 Elsevier Ltd. All rights reserved.
doi:10.1016/j.fuel.2011.11.057

Nomenclature

DMF	2,5-dimethylfuran	S_n	stretched flame propagation speed
D20	20% by volume of 2,5-dimethylfuran in *iso*-octane	T	initial temperature
E20	20% by volume of ethanol in gasoline	T_a	adiabatic flame temperature
f	laminar burning flux	u_l	laminar flame speed
L_b	Markstein length of the burned gas	α	stretch rate
M15	15% by volume of methanol in gasoline	α_T	temperature exponent
M30	30% by volume of methanol in gasoline	β_p	pressure exponent
MTBE	methyl *t*-butyl ether	δ_l	flame thickness
P	initial pressure	ρ_u	density of unburned gases
RON	research octane number	ρ_b	density of burned gases
r_u	instantaneous flame radius	σ	density ratio
SD	*standard deviation*	ν	kinematic viscosity of the unburned mixture
S_l	unstretched flame propagation speed	φ	equivalence ratio

blend at elevated temperatures and pressures over a wide range of equivalence ratios using the spherical flame method and high speed schlieren photography. The fuel blend investigated here contains 20% DMF and 80% iso-octane in volume (designated as D20).

2. Experimental setup and procedures

The details of the experimental setup are reported in previous literatures [15,17,18]. Briefly, the experimental setup consists of a combustion chamber with the heating system, a high-speed schlieren photography system, a mixture preparation system, an ignition system and a data acquisition system. The cylindrical chamber (Inner diameter: 180 mm; Volume: 5.5 l) has two quartz windows of 80 mm diameter. A Redlake HG-100 K digital camera record the flame images with a frame speed of 10,000 frames/s during the combustion.

The chamber was first heated to the required equilibrium temperature and the pre-blended liquid fuel (purity levels: DMF-99.0%, *iso*-octane-99.5%) was injected into the chamber by the micro-syringe. The required gases (purity levels: O_2-99.99%, N_2-99.99%) were introduced into the chamber according to their corresponding partial pressures. The mixtures of nitrogen and oxygen with a molar ratio of 3.76 were used to simulate air in this study. After filling, the chamber was left undisturbed for at least 5 min to ensure attainment of an approximate quiescent condition. The mixtures were ignited by the centrally located electrodes and the flame propagation was recorded by the high-speed digital camera. The chamber was then vacuumed and flushed with fresh air at least three times before next run.

The test matrix and major results (adiabatic flame temperature, density of unburned mixture, density ratio, laminar flame speed and Markstein length) of this study are summarized in Table 1. The initial pressures and temperatures were set at 0.10 MPa, 0.25 MPa, 0.50 MPa and 393 K, 433 K, 473 K, respectively, while the equivalence ratios varied from 0.9 to 1.5 in 0.1 intervals. A minimum initial temperature of 393 K was selected to ensure that D20 can be completely vaporized before the ignition (boiling points of DMF and *iso*-octane are 365 K and 372 K, respectively). The experiments were repeated twice at each condition and the average data is used in the analysis.

Table 1
Test matrix and results.

φ		0.9	1.0	1.1	1.2	1.3	1.4	1.5
P_u = 0.10 MPa, T_u = 393 K	T_a (K)	2256	2332	2344	2298	2229	2156	2083
	ρ_u(kg/m^3)	0.92	0.93	0.93	0.94	0.94	0.95	0.95
	σ	6.05	6.33	6.47	6.47	6.42	6.35	6.26
	L_b (mm)	3.92	2.36	1.98	1.54	1.03	0.57	0.02
	u_l (m/s)	0.44	0.47	0.50	0.51	0.47	0.40	0.33
P_u = 0.10 MPa, T_u = 433 K	T_a (K)	2280	2353	2367	2328	2263	2191	2119
	ρ_u(kg/m^3)	0.84	0.84	0.85	0.85	0.85	0.86	0.86
	σ	5.55	5.80	5.94	5.96	5.92	5.86	5.79
	L_b (mm)	5.38	3.31	2.2	1.82	1.79	0.74	0.1
	u_l (m/s)	0.52	0.55	0.57	0.59	0.60	0.51	0.42
P_u = 0.10 MPa, T_u = 473 K	T_a (K)	2305	2374	2391	2357	2296	2227	2157
	ρ_u(kg/m^3)	0.77	0.77	0.78	0.78	0.78	0.79	0.79
	σ	5.14	5.36	5.49	5.52	5.50	5.45	5.39
	L_b (mm)	6.1	3.46	2.2	1.92	1.8	1.02	0.59
	u_l (m/s)	0.59	0.61	0.65	0.67	0.67	0.63	0.54
P_u = 0.25 MPa, T_u = 393 K	T_a (K)	2274	2360	2365	2308	2234	2159	2085
	ρ_u(kg/m^3)	2.31	2.32	2.33	2.34	2.35	2.37	2.38
	σ	6.09	6.39	6.52	6.50	6.43	6.35	6.27
	L_b (mm)	1.13	1.08	0.76	0.75	0.28	−0.35	−0.32
	u_l (m/s)	0.31	0.35	0.42	0.44	0.40	0.32	0.31
P_u = 0.50 MPa, T_u = 393 K	T_a (K)	2286	2379	2378	2314	2237	2160	2086
	ρ_u(kg/m^3)	4.62	4.64	4.66	4.69	4.71	4.73	4.75
	σ	6.12	6.43	6.55	6.51	6.44	6.36	6.27
	L_b (mm)	0.8	0.36	0.3	0.22	−0.44	−0.49	−0.93
	u_l (m/s)	0.28	0.32	0.38	0.37	0.34	0.31	0.23

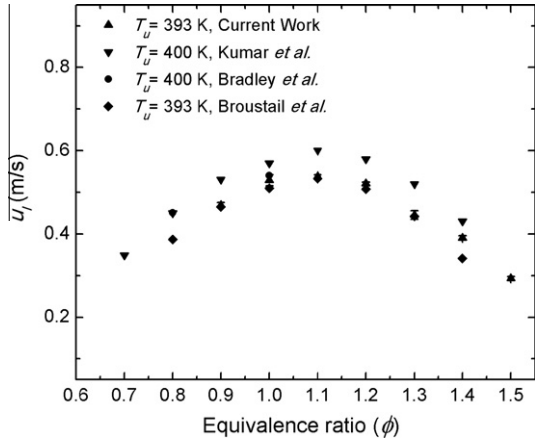

Fig. 1. Laminar flame speeds of *iso*-octane–air mixtures versus equivalence ratio at atmospheric pressure and elevated initial temperature.

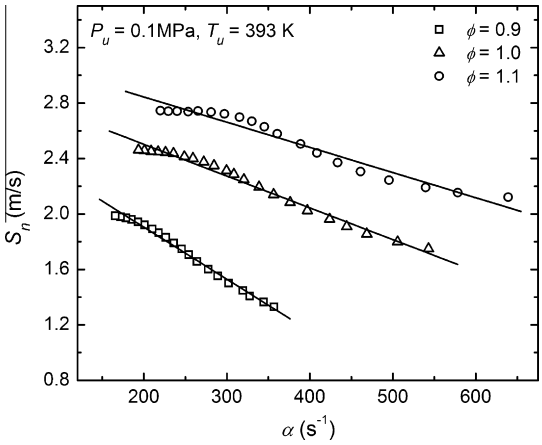

Fig. 2. Schlieren images of flames for D20–air mixtures at ambient pressure and initial temperature of 393 K for three different equivalence ratios.

3. Laminar flame speed and Markstein length

To avoid the effects of the ignition energy or the spark ignition disturbance [12,17,19–21], the pressure increase [17], the cylindrical confinement [22] and the flame-front cellular structure [23] on flame propagation, the flame images with radius between 6 mm and 25 mm are used to obtain the flame propagation speed via $S_n = dr_u/dt$. The stretch rate α is defined as $2{\cdot}S_n/r_u$ .From the linear relationship between the flame propagation speed and stretch rate [12,20,24], the unstretched flame propagation speed (S_l) can be obtained via $S_l - S_n = L_b\alpha$. By the mass conversion across the flame front, laminar flame speed can be determined via $u_l = \frac{S_l}{\sigma} = \frac{\rho_b}{\rho_u} S_l$ [12,19]. Flame thickness is calculated by the ratio of kinematic viscosity to laminar flame speed via $\delta_l = \nu/u_l$ [19]. Laminar burning flux, the eigenvalue of flame propagation, can be calculated via$f = u_l\rho_u$.

4. Results and discussions

4.1. System validation

As discussed above, no experimental or simulation data are available for laminar flame speeds of D20–air mixtures. Therefore, laminar flame speeds of *iso*-octane–air mixtures were measured and compared with data from previous literatures to validate the present measurement system. Fig. 1 shows the comparison between present measurement of laminar flame speeds of *iso*-octane–air mixtures and other open literatures such as measurements from Bradley et al. [19], Kumar et al. [25] and Broustail et al. [26]. The initial pressure for the results shown in Fig. 1 is 0.1 MPa. It is seen that present results show good agreement with the data from Refs. [19,26] because similar measurement techniques were used. Present data are slightly lower than the data of Kumar et al. [25] due to different initial temperatures and experimental methodologies. Nevertheless, the comparison shows the accuracy in measuring the laminar flame speed with the present experimental setup and methodology. The accuracy of present setup is also verified in [17,27,28] in the measurement of other fuels.

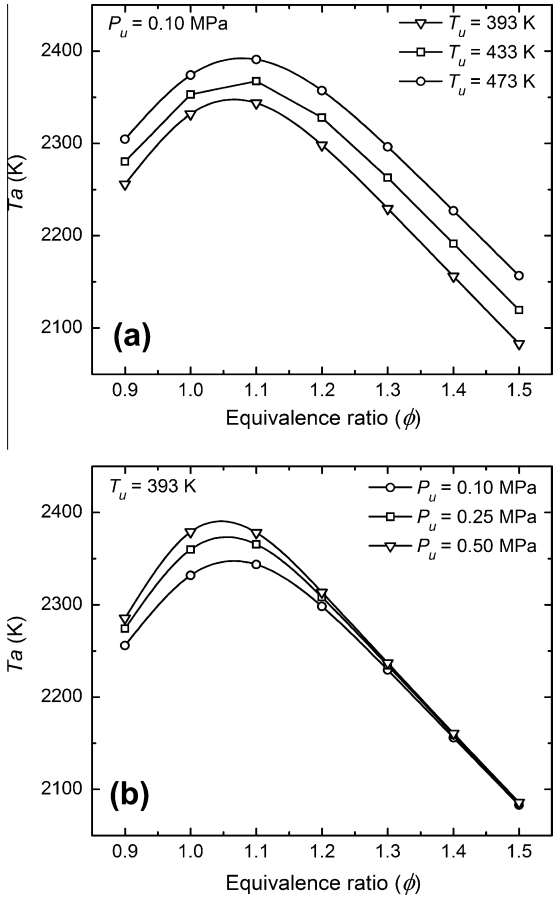

Fig. 3. Adiabatic flame temperatures of D20–air mixtures versus equivalence ratio at different initial temperatures (a) and pressures (b).

4.2. Flame propagation

Fig. 2 shows the stretched flame propagation speed of D20–air mixtures versus stretch rate at three different equivalence ratios under the corresponding initial condition. The stretched flame propagation speed shows a linear relationship with the stretch rate. The stretched flame propagation speed decreases with the increase of stretch rate (decrease of flame radius) which means Markstein length takes the positive value, as shown in Table 1. The slope of S_n–α curve increases with the increase of equivalence ratio.

4.3. Laminar flame parameters

Adiabatic flame temperature is an important parameter for the combustion phenomena. It has a close relationship to NO_x

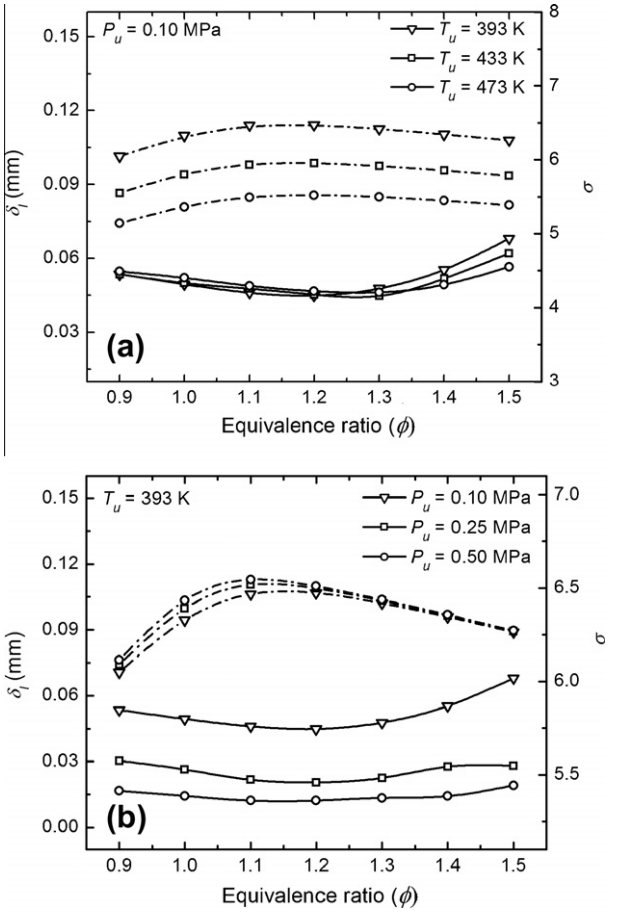

Fig. 4. Flame thicknesses (solid line) and density ratios (dash dot line) of D20–air mixtures versus equivalence ratio at different initial temperatures (a) and pressures (b).

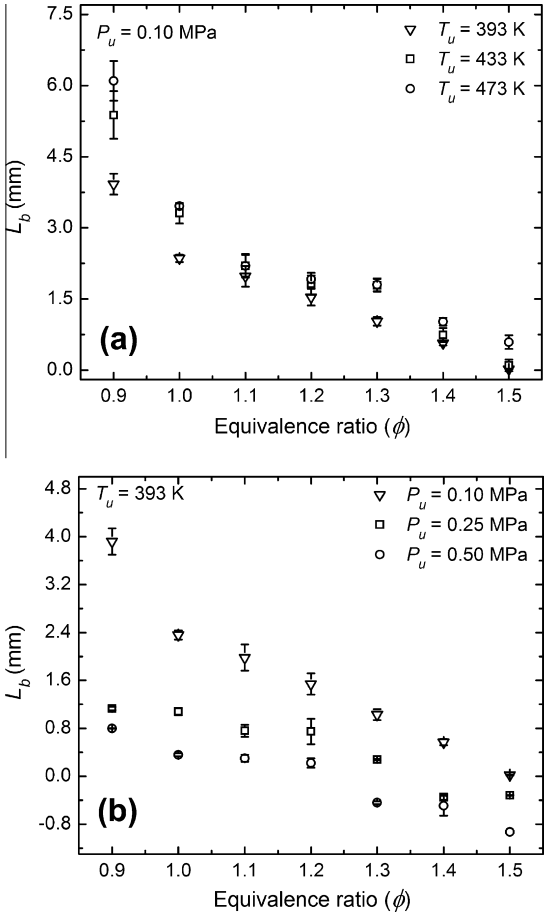

Fig. 5. Markstein lengths of D20–air mixtures versus equivalence ratio at different initial temperatures (a) and pressures (b).

formation and laminar flame speed due to its effect on species equilibrium and heat/mass diffusion of the flame front [29–31]. In this study, the adiabatic flame temperature is calculated using the method described in [32,33]. Adiabatic flame temperatures of D20–air mixtures versus the equivalence ratio at different initial temperatures and pressures are shown in Fig. 3. The adiabatic flame temperature peaks near an equivalence ratio of 1.1 due to the product dissociation and reduced amount of heat release [34]. With the increase of initial temperature, the adiabatic flame temperature increases. Since the amount of dissociation decreases with the increase of initial pressure, the adiabatic flame temperature should be higher at higher pressure [31]. As shown in Fig. 3b, the adiabatic flame temperature increases with the increase of initial pressure when the equivalence ratio is less than 1.2. The influence of initial pressure on adiabatic flame temperature is quite moderate on the rich mixture side.

Flame thickness and density ratio are the controlling parameters of the hydrodynamic instability. Increase in density ratio or decreasing in flame thickness promotes the hydrodynamic instability [35–37]. Fig. 4 shows the flame thicknesses and density ratios of D20–air mixtures versus equivalence ratio at different initial temperatures and pressures. The flame thickness decreases with the increase of initial pressure and is insensitive to the variation of initial temperature, while the density ratio decreases with the increase of initial temperature and slightly increases with the increase of initial pressure. Therefore, the hydrodynamic instability of D20–air mixtures decreases with increasing initial temperature but increases with increasing initial pressure.

Based on the asymptotic theory [38], Markstein length depends on the Lewis number of fuel (lean mixture) or oxidizer (rich mixture). For hydrogen and light hydrocarbon–air mixtures, Markstein length increases with the increase of equivalence ratio; while for heavy hydrocarbon–air mixtures, it decreases with the increase of equivalence ratio [39]. Since DMF and *iso*-octane are both heavy hydrocarbon fuels, Markstein length of D20 should decrease with the increase of equivalence ratio. Fig. 5 shows the Markstein length of D20–air mixtures versus equivalence ratio at different initial temperatures and pressures. Markstein length decreases with the increase of equivalence ratio under all conditions in this study, and it increases with increasing initial temperature but decreases with increasing initial pressure. This trend is similar to that of DMF as reported in [13,14]. This means that at a lower initial temperature and higher initial pressure, the flame propagation is less affected by the flame stretch rate and the flames of the D20–air mixtures are less stable, especially for the rich mixtures. Values of laminar flame speeds and Markstein lengths depends on extrapolation model and this dependence is more significant for non-unity Lewis number mixtures, as reported in Refs. [40,41]. The linear extrapolation model used in this study might be over-predicted laminar flame speed and Markstein length when Markstein length is large (Lewis number is non-unity). Thus, laminar flame speed and Markstein length of D20–air mixture in this study might be larger than the true value due to the limitation and character of the linear extrapolation mode. As shown in Fig. 6, cracks can be observed on the flame front when flame radius is larger than 20 mm. Meanwhile, postponing of crack appearance on the

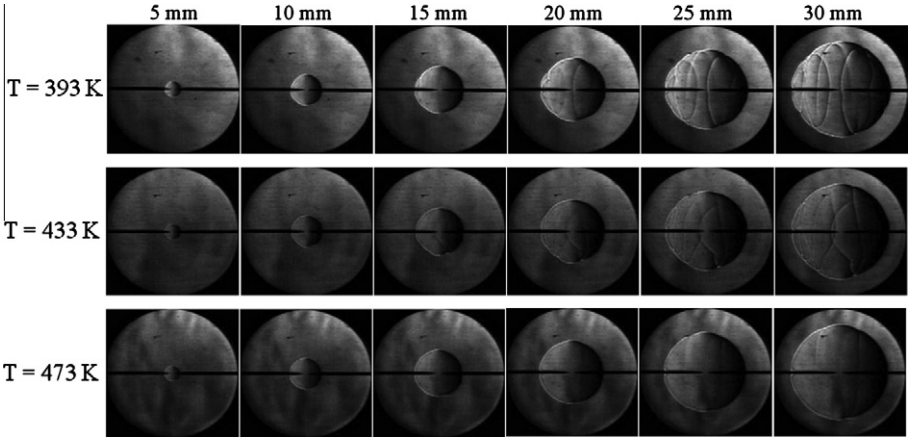

Fig. 6. Schlieren images of flames for D20–air mixtures at the ambient pressure and the equivalence ratio of 1.5 at three different initial temperatures.

flame front is presented as the initial temperature increases due to the increase of Markstein length with increasing initial temperature. Schlieren images of flames for D20–air mixtures at three different initial pressures are shown in Fig. 7. For initial pressures of 0.10 and 0.25 MPa, the flame front keeps smooth without cracks even when the flame radius is 30 mm. However, at the initial pressure of 0.50 MPa, cracks appear on the flame front when flame radius is only 10 mm. Cracks have developed into cellular structures when the flame radius is 30 mm at the same condition. This is due to the combined effect of diffusional-thermal and hydrodynamic instabilities. As discussed above, Markstein length and flame thickness decreases with the increase of initial pressure. The increased hydrodynamic instability cannot be stabilized by the decreased diffusional-thermal stability.

Fig. 8 shows laminar flame speed and laminar burning flux of D20–air mixtures versus equivalence ratio at different initial temperatures and pressures. Laminar flame speed strongly depends on the initial condition and we empirically correlated the burning velocities with temperature and pressure, as

$$u_l = u_{l0}\left(\frac{T_u}{T_{u0}}\right)^{\alpha_T}\left(\frac{P_u}{P_{u0}}\right)^{\beta_P} \tag{1}$$

where subscript '0' refers to the reference condition. In this study, P_{u0} = 0.1 MPa, T_{u0} = 393 K. α_T and β_P are the exponents of temperature and pressure, respectively.

Eq. (5) can be simplified as temperature and pressure dependent,

$$u_l = u_{l0}\left(\frac{T_u}{T_{u0}}\right)^{\alpha_T} \tag{2}$$

$$u_l = U(P_u)^{\beta_P} \tag{3}$$

Based on the method described in literatures [13,14], u_{l0} and α_T *are* correlated as following:

$$u_{l0} = 7.486\phi^4 - 36.504\phi^3 + 64.68\phi^2 - 49.41\phi + 14.215 \tag{4}$$

$$\alpha_T = -50.671\phi^4 + 227.45\phi^3 - 370.26\phi^2 + 259.36\phi - 64.389 \tag{5}$$

The values of U and β_P are shown in Table 2.

As shown in Fig. 8, laminar flame speeds peak near an equivalence ratio of 1.2. The peak position moves slightly to the rich mixture side with the increase of initial temperature. Laminar flame speed increases with the increase of initial temperature and decreases with the increase of initial pressure. The laminar burning flux increases with the increase of initial temperature and pressure. Both laminar flame speed and the density of the unburned mixture vary with initial temperature and pressure. With the increase of initial temperature, the increase of laminar flame speed is dominant over the decrease of the density of the unburned mixture. Meantime, the increasing density of the unburned mixture with the increase of initial pressure is more obvious compared to the reduction of the laminar flame speed. Thus, the combined

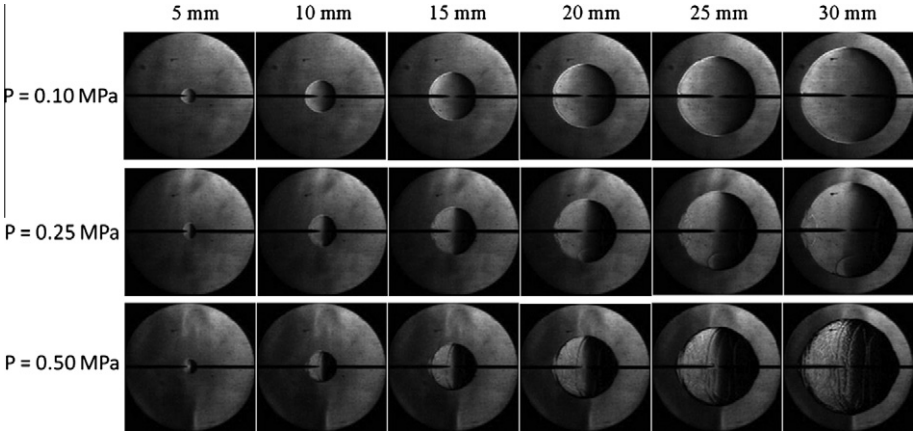

Fig. 7. Schlieren images of flames for D20–air mixtures at the equivalence ratio of 1.2 and the initial temperature of 393 K at three different initial pressures.

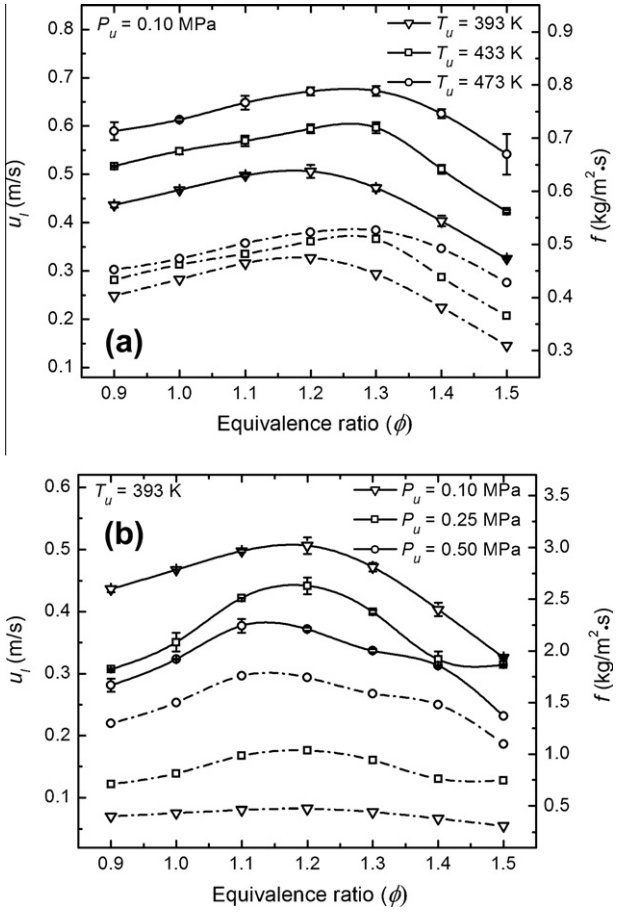

Fig. 8. Laminar flame speed (solid line) and laminar burning flux (dash dot line) of D20–air mixtures versus equivalence ratio at different initial temperatures (a) and pressures (b).

effects of these two aspects contribute to the increase of the laminar burning flux with the initial temperature and pressure.

Fig. 9 shows laminar flame speed of different fuels versus equivalence ratio at atmospheric pressure. The results show that the laminar flame speeds of *iso*-octane–air mixtures are higher than those of the DMF–air mixtures at equivalence ratio less than 1.1 and but lower at equivalence ratio larger than 1.1. The peak value of laminar flame speed for *iso*-octane is presented at equivalence ratio of 1.1 while the laminar flame speed of DMF and D20 give their peak at equivalence ratio of 1.2. The possible reason is that the oxygen in the fuel will promote the reaction rate at rich mixture side. Thus, adding DMF into *iso*-octane may increase the laminar flame speeds. This effect is obvious only when the equivalence ratio is greater than 1.2 where D20 has a higher laminar flame speed than *iso*-octane. When the equivalence ratio is less than 1.2, the laminar flame speed of D20 is lower than that of *iso*-octane. In Ref. [42], the blends of methanol and *iso*-octane gave lower laminar flame speed than both pure fuels. This is mainly due to the chain transfer between alkyl radicals and formaldehyde formed

Table 2
Values of U and β_P.

φ	0.9	1.0	1.1	1.2	1.3	1.4	1.5
U_l	0.42	0.46	0.50	0.51	0.48	0.39	0.34
β_P	−0.279	−0.233	−0.173	−0.190	−0.208	−0.162	−0.204
SD (m/s)	0.006	0.005	0.001	0.003	0.002	0.005	0.010

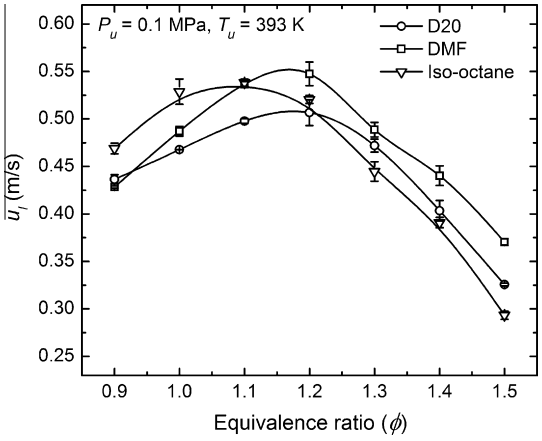

Fig. 9. Comparison of laminar burning velocities for different fuels at elevated initial temperature and ambient pressure.

during oxidation which reduces the reaction rate. Reported data of ethanol/butanol and *iso*-octane blends showed that laminar flame speeds of the fuel mixture were higher than pure *iso*-octane, but lower than pure ethanol/butanol [26]. In Ref. [19], the results showed that *iso*-octane and 90% *iso*-octane/10% n-heptane–air mixtures have similar laminar flame speeds. In [43], the laminar flame speeds of M15 and M30 (15% an 30% methanol in gasoline by volume, respectively) at the equivalence ratio of 1.3 is larger than that of gasoline and methanol. The inhibition and/or promotion mechanism resulting from blending two different fuels contributes to the decrease and/or the increase of laminar flame speed. Detailed chemical kinetics of DMF, which is currently unavailable, coupled with the chemical kinetics of *iso*-octane will help to explain the phenomenon observed in this study.

5. Conclusions

Laminar combustion characteristics of D20–air mixtures were studied at elevated temperatures and pressures over wide range of equivalence ratios. The main conclusions are summarized as follows:

(1) Laminar flame speed of D20–air premixed mixtures peaks near an equivalence ratio of 1.2. It increases with increasing initial temperature and decreasing the initial pressure.
(2) Adiabatic flame temperature peaks near the equivalence ratio of 1.1 due to the product dissociation and reduced amount of heat release. The adiabatic flame temperature increases with the increase of initial temperature and is insensitive to initial pressure at rich mixture side.
(3) Markstein length decreases with the increase of equivalence ratio and initial pressure, while it increases with the increase of initial temperature. Cellular structures appear at rich mixture flame front of D20–air mixture at high initial pressure due to the combined effect of diffusional-thermal and hydrodynamic instabilities.
(4) Laminar burning flux peaks near an equivalence ratio of 1.2 and increases with the increase of initial temperature and pressure.
(5) Adding small ratio of DMF into *iso*-octane will increase laminar flame speed when the equivalence ratio is greater than 1.2 and decrease laminar flame speed at equivalence ratio less than 1.2, compared to the laminar flame speed of *iso*-octane.

Acknowledgment

This work is supported by the National Natural Science Foundation of China (Nos. 50876085, 51136005).

References

[1] Román-Leshkov Y, Barrett CJ, Liu ZY, Dumesic JA. Production of dimethylfuran for liquid fuels from biomass-derived carbohydrates. Nature 2007;447:982–5.
[2] Zhao H, Holladay JE, Brown H, Zhang ZC. Metal chlorides in ionic liquid solvents convert sugars to 5-hydroxymethylfurfural. Science 2007;316:1597–600.
[3] Mascal M, Nikitin EB. Direct high-yield conversion of cellulose into biofuel. Angew Chem Int Edit 2008;47:7924–6.
[4] Mousdale DM. Biofuels: biotechnology, chemistry, and sustainable development. UK: Taylor & Francis Group, CRC Press; 2008
[5] Grela MA, Amorebieta VT, Colussi AJ. Very low pressure pyrolysis of furan, 2-methylfuran and 2, 5-dimethylfuran. The stability of the furan ring. J Phys Chem 1985;89:38–41.
[6] Lifshitz A, Tamburu C, Shashua R. Thermal decomposition of 2, 5-dimethylfuran. Experimental results and computer modeling. J Phys Chem Part A 1998;102:10655–70.
[7] Jiao CQ, Adams SF, Garscadden A. Ionization of 2, 5-dimethylfuran by electron impact and resulting ion-parent molecule reactions. J Appl Phys 2009;106:4.
[8] Wu X, Huang Z, Yuan T, Zhang K, Wei L. Identification of combustion intermediates in a low-pressure premixed laminar 2, 5-dimethylfuran/oxygen/argon flame with tunable synchrotron photoionization. Combust Flame 2009;156:1365–76.
[9] Zhong S, Daniel R, Xu H, Zhang J, Turner D, Wyszynski ML, et al. Combustion and emissions of 2, 5-Dimethylfuran in a direct-injection spark-ignition engine. Energy Fuels 2010;24:2891–9.
[10] Daniel R, Tian G, Xu H, Wyszynski ML, Wu X, Huang Z. Effect of spark timing and load on a DISI engine fuelled with 2, 5-dimethylfuran. Fuel 2011;90:449–58.
[11] Wu X, Daniel R, Tian G, Xu H, Huang Z, Richardson D. Dual-injection: the flexible. Bi-fuel concept for spark-ignition engines fuelled with various gasoline and biofuel blends. 2011;88:2305–14.
[12] Law CK, Sung CJ. Structure, aerodynamics, and geometry of premixed flamelets. Prog Energy Combust Sci 2000;26:459–505.
[13] Wu X, Huang Z, Wang X, Jin C, Tang C, Wei L, et al. Laminar burning velocities and flame instabilities of 2, 5-dimethylfuran–air mixtures at elevated pressures. Combust Flame 2011;158:539–46.
[14] Wu X, Huang Z, Jin C, Wang X, Wei L. Laminar burning velocities and Markstein lengths of 2, 5-dimethylfuran–air premixed flames at elevated temperatures. Combust Sci Technol 2011;183:220–37.
[15] Wu X, Huang Z, Jin C, Wang X, Zheng B, Zhang Y, et al. Measurements of laminar burning velocities and Markstein lengths of 2, 5-dimethylfuran–air-diluent premixed flames. Energy Fuels 2009;23:4355–62.
[16] Tian G, Daniel R, Li H, Xu H, Shuai S, Richards P. Laminar burning velocities of 2, 5-dimethylfuran compared with ethanol and gasoline. Energy Fuels 2010;24:3898–905.
[17] Zhang Z, Huang Z, Wang X, Xiang J, Wang X, Miao H. Measurements of laminar burning velocities and Markstein lengths for methanol–air–nitrogen mixtures at elevated pressures and temperatures. Combust Flame 2008;155:358–68.
[18] Tang C, Huang Z, Jin C, He J, Wang J, Wang X. Laminar burning velocities and combustion characteristics of propane–hydrogen–air premixed flames. Int J Hydrogen Energy 2008;33:4906–14.
[19] Bradley D, Hicks RA, Lawes M, Sheppard CGW, Woolley R. The measurement of laminar burning velocities and Markstein numbers for iso-octane–air and iso-octane-n-heptane–air mixtures at elevated temperatures and pressures in an explosion bomb. Combust Flame 1998;115:126–44.
[20] Chen Z, Burke MP, Ju Y. Effects of Lewis number and ignition energy on the determination of laminar flame speed using propagating spherical flames. Proc Combust Inst 2009;32:1253–60.
[21] Huang Z, Zhang Y, Zeng K, Liu B, Wang Q, Jiang D. Measurements of laminar burning velocities for natural gas–hydrogen–air mixtures. Combust Flame 2006;146:302–11.
[22] Burke MP, Chen Z, Ju Y, Dryer FL. Effect of cylindrical confinement on the determination of laminar flame speeds using outwardly propagating flames. Combust Flame 2009;156:771–9.
[23] Bradley D, Lawes M, Liu K, Verhelst S, Woolley R. Laminar burning velocities of lean hydrogen–air mixtures at pressures up to 1.0 MPa. Combust Flame 2007;149:162–72.
[24] Gu XJ, Haq MZ, Lawes M, Woolley R. Laminar burning velocity and Markstein lengths of methane–air mixtures. Combust Flame 2000;121:41–58.
[25] Kumar K, Freeh JE, Sung CJ, Huang Y. Laminar flame speeds of preheated iso-octane/O_2/N_2 and n-heptane/O_2/N_2 mixtures. J Propul Power 2007;23:428–36.
[26] Broustail G, Seers P, Halter F, Moréac G, Mounaim-Rousselle C. Experimental determination of laminar burning velocity for butanol and ethanol iso-octane blends. Fuel 2011;90:1–6.
[27] Tang C, Huang Z, He J, Jin C, Wang X, Miao H. Effects of N_2 dilution on laminar burning characteristics of propane–air premixed flames. Energy Fuels 2009;23:151–6.
[28] Gu X, Huang Z, Wu S, Li Q. Laminar burning velocities and flame instabilities of butanol isomers–air mixtures. Combust Flame 2010;157:2318–25.
[29] Bowman CT. Kinetics of pollutant formation and destruction in combustion. Prog Energy Combust Sci 1975;1:33–45.
[30] Simon DM. Flame propagation. III. Theoretical consideration of the burning velocities of hydrocarbons 1. J Am Chem Soc 1951;73:422–5.
[31] Law CK. Combustion physics. 1st ed. Cambridge: Cambridge University Press; 2006.
[32] Turns SR. An introduction to combustion concepts and applications. Singapore: McGraw–Hill; 1999.
[33] Olikara C, Borman GL. A computer program for calculating properties of equilibrium combustion products with some applications to I.C. Engines. SAE 1975;750468.
[34] Law CK, Makino A, Lu TF. On the off-stoichiometric peaking of adiabatic flame temperature. Combust Flame 2006;145:808–19.
[35] Kwon OC, Rozenchan G, Law CK. Cellular instabilities and self-acceleration of outwardly propagating spherical flames. Proc Combust Inst 2002;29:1775–83.
[36] Rozenchan G, Zhu DL, Law CK, Tse SD. Outward propagation, burning velocities, and chemical effects of methane flames up to 60 ATM. Proc Combust Inst 2002;29:1461–70.
[37] Jomaas G, Law CK, Bechtold JK. On transition to cellularity in expanding spherical flames. J Fluid Mech 2007;583:1–26.
[38] Matalon M, Matkowsky BJ. Flames as gas dynamic discontinuities. J Fluid Mech 1982;124:239–59.
[39] Bechtold JK, Matalon M. The dependence of the Markstein length on stoichiometry. Combust Flame 2001;127:1906–13.
[40] Chen Z. On the extraction of laminar flame speed and Markstein length from outwardly propagating spherical flames. Combust Flame 2011;158:291–300.
[41] Kelley AP, Law CK. Nonlinear effects in the extraction of laminar flame speeds from expanding spherical flames. Combust Flame 2009;156:1844–51.
[42] Gulder ÖL. Laminar burning velocities of methanol, isooctane and isooctane/methanol blends. Combust Sci Technol 1983;33:179–92.
[43] Liao SY, Jiang DM, Cheng Q, Huang ZH, Zeng K. Effect of methanol addition into gasoline on the combustion characteristics at relatively low temperatures. Energy Fuels 2006;20:84–90.